European Cells and Materials Vol. 46 2023 (pages 1-23) DOI: 10.22203/eCM.v046a01 ISSN 1473-2262

CREATING TISSUE WITH INTERVERTEBRAL DISC-LIKE CHARACTERISTICS USING GDF5 FUNCTIONALIZED SILK SCAFFOLDS AND HUMAN MESENCHYMAL STROMAL CELLS

A.S. Croft[1,2,*], J. Fuhrer[1], M. Wöltje[3] and B. Gantenbein[1,4]

[1] Tissue Engineering for Orthopaedic & Mechanobiology, Bone & Joint Program, Department for BioMedical Research (DBMR), Medical Faculty, University of Bern, CH-3008 Bern, Switzerland
[2] Graduate School for Cellular and Biomedical Sciences (GCB), University of Bern, CH-3012 Bern, Switzerland
[3] Institute of Textile Machinery and High Performance Material Technology, TUD University of Technology, Dresden, Hohe Str. 6, 01069 Dresden, Germany
[4] Department of Orthopaedic Surgery & Traumatology, Inselspital, Bern University Hospital, Medical Faculty, University of Bern, CH-3010 Bern, Switzerland

Abstract

For years, researchers have searched for a suitable biomaterial to regenerate the intervertebral disc (IVD). A promising candidate is silk, as there have been several approaches in the past where silk fibroin was used to repair the IVD's nucleus pulposus (NP) and annulus fibrosus (AF). However, to date, nobody has attempted to recreate IVD tissue with dimensions and cell densities comparable to a human IVD using silk and human mesenchymal stromal cells (MSC). Therefore, silk scaffolds were produced from *Bombyx mori* yarn. To mimic the AF, the yarn was embroidered into a ring-like structure or patch. To mimic the NP, fibre-additive manufacturing was applied to create highly porous constructs. Half of the NP scaffolds were functionalized with the growth differentiation factor 5 (GDF5). The scaffolds were seeded with MSCs from five human donors in a density of one-third of the density found in the human IVD and cultured for 7, 14 or 21 days in transforming growth factor β1 (TGF-β1)-enriched medium. All scaffolds were biocompatible as cell numbers increased by a factor 4-5. Furthermore, the scaffolds generally showed an anabolic phenotype, which was positively influenced by GDF5, and tissue-like characteristics were promoted based on the scaffolds' morphology. In conclusion, the here proposed silk scaffolds showed IVD-like characteristics with a size and cell density comparable to human IVD tissue.

Keywords: Silk, *Bombyx mori*, intervertebral disc, growth and differentiation factor 5, mesenchymal stromal cells, scaffolds, nucleus pulposus regeneration, annulus fibrosus regeneration.

***Address for correspondence**: Andreas S. Croft, Tissue Engineering for Orthopaedics & Mechanobiology (TOM), Bone & Joint Program, Department for BioMedical Research (DBMR), Medical Faculty, University of Bern, Murtenstrasse 35, 3008, Bern, Switzerland
Telephone number: +41 31 632 98 83 Email: andreas.croft@unibe.ch

List of Abbreviations

α-MEM	α-minimal essential medium
ACAN	aggrecan
ADAMTS4	ADAM metallopeptidase with thrombospondin type 1 motif 4
AF	annulus fibrosus
CD24	cluster of differentiation 24
CD146	cluster of differentiation 146
COL1	collagen type 1
COL2	collagen type 2
COL10	collagen type 10
DABA	4-dimethylamino-benzaldehyd
ECM	extracellular matrix
EDC	N-ethyl-N-(3-dimethylaminopropyl)carbodiimide hydrochloride
FAM	fibre-additive manufacturing
FBLN1	fibulin 1
FBS	fetal bovine serum
FGF2	fibroblast growth factor 2
GAG	glycosaminoglycan
GAPDH	glyceraldehyde-3-phosphate dehydrogenase
GDF5	growth differentiation factor 5
GDF6	growth differentiation factor 6
HYP	hydroxyproline
IBSP	integrin binding sialoprotein
IDD	intervertebral disc degeneration
ITS	insulin, transferrin, selenium
IVD	intervertebral disc
KRT8	cytokeratin 8
KRT19	cytokeratin 19
LBP	low back pain
LG-DMEM	low-glucose Dulbecco's Modified Eagle Medium
MES	2-(N-morpholino) ethanesulfonic acid
MMP13	matrix metallopeptidase 13
MSC	mesenchymal stromal cell
NHS	N-hydroxysuccinimide
Nm	number metric
NP	nucleus pulposus
PBS	phosphate buffered saline
qPCR	quantitative polymerase chain reaction
SEM	scanning electron microscope
SF	silk fibroin
SOX9	SRY-box transcription factor 9
TGF-β1	transforming growth factor β1

Introduction

With a global one-year prevalence of up to 40 %, low back pain (LBP) affects a large number of people worldwide and produces immense costs for the health care system and burdens the economy due to loss of working force (Dagenais *et al.*, 2008; Hoy *et al.*, 2012). In 2020, an estimated 600 M patients suffered from LBP and latest numbers prognose an increase of 200 M patients by 2050 (Ferreira *et al.*, 2023). The causes of LBP are diverse: from muscular issues and systemic diseases to fractures (Deyo and Weinstein, 2001). Although exact mechanisms have yet to be discovered, intervertebral disc (IVD) degeneration (IDD) is highly correlated with unspecific LBP and is thought to be the strongest contributor to the problem (Brinjikji *et al.*, 2015). The first signs of IDD usually appear in the IVD's highly hydrated and collagen type II (COL2) rich core tissue, the nucleus pulposus (NP) (Adams and Roughley, 2006). To keep the NP in place, it is surrounded by a more resilient and collagen type I (COL1) rich tissue, the annulus fibrosus (AF) (Inoue and Takeda, 1975). During IDD, the IVD tissue is characterized by an increased rate of cell death and a subsequent decreased extracellular matrix (ECM) synthesis due to an overactivity of catabolic processes that are mainly mediated by metalloproteinases and aggrecanases (Eyre and Muir, 1976; Oichi *et al.*, 2020). Consequently, the IVD's height diminishes as the NP loses its water binding capacity and morphological changes like fissures appear within the AF, which can induce disc herniation (Oichi *et al.*, 2020).

An emerging field to treat IDD is tissue engineering, as scaffolds, cells, and biologically active molecules can be combined to restore tissue or to create tissue-like structures (Berthiaume *et al.*, 2011). A promising candidate for IVD tissue engineering is silk harvested from the silkworm *Bombyx mori* Linnaeus, 1758 (Bhunia *et al.*, 2018). Especially the silk's structural core protein, silk fibroin (SF), fulfils all the important requirements for an optimal biomaterial. It displays a low immunogenicity,

great biocompatible and mechanical properties, adaptable biodegradation, and versatile structural and chemical modifications like functionalization are possible (Altman *et al.*, 2003; Yang *et al.*, 2020). Especially the latter makes SF very attractive for tissue engineering, as cytokines and growth factors can be conjugated to the SF's side chains, enabling a long-term supply or controlled release of certain molecules to enhance the tissue-specific biological properties of the scaffold (Croft *et al.*, 2022). An interesting molecule that has received increasing attention in IDD-related therapy is growth differentiation factor 5 (GDF5) (Lv *et al.*, 2022). GDF5 has been correlated with IVD growth and homeostasis, as it can increase the proteoglycan content in the NP and restore the IVD's height (Chujo *et al.*, 2006). Furthermore, studies have demonstrated that GDF5 can be used to differentiate human mesenchymal stromal cells (MSC) towards NP-like cells, especially when GDF5 is combined with transforming growth factor β1 (TGF-β1) (Colombier *et al.*, 2016; Gantenbein-Ritter *et al.*, 2011). This tissue-specific differentiation of MSCs is essential, otherwise the chances are low that the un- or incorrectly conditioned cells would successfully adapt and survive long-term in the distinct and harsh environment of the IVD (Wuertz *et al.*, 2009; Wuertz *et al.*, 2008). The difficulty here is to guide the differentiation of the MSCs towards an NP or AF cell-like phenotype instead of a general chondrogenic phenotype (Colombier *et al.*, 2016). Over time, a series of molecular markers have been identified to distinguish NP, AF cells and chondrocytes from each other, including *cytokeratin 19 (KRT19)*, *cytokeratin 8 (KRT8)*, *cluster of differentiation 24 (CD24)*, *aggrecan (ACAN)* and *COL2* for NP cells and *cluster of differentiation 146 (CD146)*, *fibulin 1 (FBLN1)*, *integrin binding sialoprotein (IBSP)*, and *COL1* for AF cells, respectively (Du *et al.*, 2022; Minogue *et al.*, 2010; Peng *et al.*, 2021; Risbud *et al.*, 2015). Apart from the chemical cues of the growth factors, the morphology of the culture substrate itself is also known to influence the cell's fate. For example, AF cells that are cultured on a scaffold with lamellar features like native AF tissue better maintain an AF-like phenotype than the cells cultured on a porous scaffold that is morphologically less similar to native AF tissue (Nerurkar *et al.*, 2009; Park *et al.*, 2012b). Hence, previous studies have suggested that MSCs cultured on softer substrates are more likely to differentiate towards an NP-like phenotype, whereas stiffer substrates are more likely to promote an AF-like phenotype (Feng *et al.*, 2020; Peng *et al.*, 2021). In this context, multiple studies have specifically used silk as a scaffold or hydrogel to repair the IVD or to promote the synthesis of NP-like or AF-like tissue (Croft *et al.*, 2022). However, cell densities similar to what can be found in human NP or AF tissue have often been neglected (Zeng *et al.*, 2014; Zhang *et al.*, 2020) or no cells were incorporated at all (Frauchiger *et al.*, 2018b; Hu *et al.*, 2017). Moreover, virtually all silk-based IVD scaffolds from previous studies have been scaled down considerably, corresponding to only a fraction of the actual IVD tissue in the human body (Bhattacharjee *et al.*, 2012; Park *et al.*, 2012a; Zeng *et al.*, 2014). So far, the only study that aimed to create IVD tissue with an entire human-sized structure using SF was conducted by Costa *et al.* (2019). Here, they reverse-engineered AF tissue based on an MRI scan of a human IVD and 3D printed the scaffold at a 1:1 scale. However, the *in vitro* study did not assess any IVD-cell like differentiation.

With all that in mind, we hypothesized whether human NP- and AF-like tissue could be made by combining functionalized silk scaffolds designed to morphologically mimic NP and AF tissue with human bone marrow-derived MSCs cultured in TGF-β1-enriched chondrogenic inductive medium. Moreover, we hypothesized that the morphology of the silk scaffolds on its own could promote tissue-specific differentiation and that the differentiation could be further enhanced when adding GDF5. Therefore, we aimed to create tissue with NP- and AF-like characteristics with a size and cell density comparable to what can be found in a physiological human IVD.

Materials and Methods

Silk scaffolds

The silk scaffolds were fabricated as previously described (Wöltje *et al.*, 2023). In brief, the fabrication of the silk scaffolds went as follows:

NP scaffolds

The NP scaffolds were made of Grège silk yarn (40/42 den; Plauener Seidenweberei GmbH, Plauen, Germany), which were cut into short fibres with a length of 1 mm. For the assembly of the textile NP structure with an average porosity of 94 %, fibre-additive manufacturing (FAM) was used. FAM is a solid free forming approach where textile fibres are processed into 3D non-woven structures without the need for negative moulds, or forging dies (Hild *et al.*, 2014). Here, the creation of the NP scaffolds included the following steps: (i) a layer of anisotropic silk fibres was deposited, (ii) regenerated SF adhesive was spread spatially over the silk fibres drop by drop, (iii) a new silk fibre layer was placed on top, which was bonded to the previous layer by the SF adhesive. After each manufactured layer, the fabrication slide was moved down by the thickness of one layer. This process was then repeated until the desired dimensions (diameter = 15 mm, height = 3 mm) of the scaffold was achieved (Fig. 1**a**).

Once manufactured, half of the NP scaffolds were functionalized with GDF5.

Functionalization of NP scaffolds

First, the NP scaffolds were disinfected with 70 % EtOH for 30 minutes. Then, the EtOH was aspirated and the scaffolds were washed three times with sterile ddH_2O. The scaffolds were then dried in a clean bench. All subsequent work was performed aseptically under a clean bench only. For functionalization by carbodiimide chemistry, the NP scaffolds were first placed in 0.1 M 2-(N-morpholino) ethanesulfonic acid (MES) buffer (Carl Roth GmbH + Co. KG, Karlsruhe, Germany; #4256.2) for 30 minutes and the buffer was then aspirated. This was followed by activation of the carboxyl groups of the amino acids aspartic acid and glutamic acid of the fibroin molecules of the silk yarn. For this purpose, a 5.2 mM N-ethyl-N-(3-dimethylaminopropyl) carbodiimide hydrochloride (EDC; Pierce/Fisher Scientific, Schwerte, Germany; #PG82073) and a 12.16 mM N-hydroxysuccinimide (NHS; Merck KGaA, Darmstadt, Germany; #56485) solution were prepared in MES immediately before use, mixed in a 1:1 ratio, and added to the NP scaffolds. After 15 minutes, the EDC-NHS solution was aspirated and the activated NP scaffolds were incubated with 400 ng GDF5 (PreproTech, Hamburg, Germany; #120-01) each for 1 hour at room temperature. Then, the solution was aspirated from the scaffolds and washed three times with phosphate buffered saline (PBS) intensively. Finally, the scaffolds functionalized with GDF5 were dried inside the clean bench at room temperature and stored after drying at 4 °C until use.

Despite the interconnecting pore structure, direct quantification of covalently bound GDF5 molecules using GDF5 antibodies as used for ELISAs was difficult because a complete washout of unbound detection antibodies could not be guaranteed. Therefore, a reporter enzyme (alkaline phosphatase) was covalently coupled to the silk scaffold using carbodiimide chemistry. A calibration curve was used to correlate the substrate turnover with the coupled enzyme amount. The coupling efficiency achieved here was 30.7 %. In addition, the experiment showed that the EDC/NHS chemistry does not affect the bioactivity of the coupled protein (data not shown). Under the same experimental conditions for the coupling of the GDF5 to the FAM scaffold and the premise of the same coupling efficiency, this results in a GDF5 amount per scaffold of 122.8 ng for an initial GDF5 amount of 400 ng per scaffold.

Furthermore, to determine that no covalently bound GDF5 was released during the culture period, one non-functionalized NP Control scaffold and one GDF5-functionalized NP scaffold were incubated for 24 days in PBS. The PBS was collected every three to four days and replaced with fresh PBS. After 24 days, the amount released GDF5 was measured from every timepoint following the instruction manual of a GDF5 ELISA kit (Cloud-Clone Corporation, Houston, USA; #SEC110Hu).

AF samples

For the AF scaffolds, a twisted schappe silk yarn (Plauener Seidenweberei GmbH, Plauen, Germany) with a fineness 140/2 Nm (number metric) was used. This silk yarn was then embroidered into a ribbon, which contained four layers of yarn and based on the natural structure of the AF, each layer was embroidered with an alternating orientation of – 30 ° and + 30 ° (ZSK Racer 1W, Stickmaschinen GmbH, Krefeld,

Germany). The distance of the yarn deposit was set at 0.7 mm, and the silk yarn in each layer was embroidered on the water-soluble embroidery ground (Gunold GmbH, Stockstadt, Germany, #41825). After embroidery, the silk ribbons were removed from the embroidery ground using a two-step washing procedure and then dried. Once dried, the ribbon was assembled by winding it into a snail-like shape. Like this, the AF scaffold consisted of a total of 16 fibre layers, a diameter of 35 mm and a height of 8 mm (Fig. 1**c**). Finally, to prevent the scaffold from unwinding itself, the ribbon was fixed at two positions by manual stitching.

However, due to the size of the AF scaffolds and the resulting cell numbers needed for seeding (20 million cells per scaffold), high numbers of replicates for all conditions were not feasible due to logistical reasons, meaning that only data for day 0 and day 21 could be collected for the AF scaffolds. To compensate for this issue, 8 × 8 mm big AF patches were cut from an AF scaffold (Fig. 1**b**). With these AF patches, it was then possible to analyze all four time points and not just day 0 and day 21. Since the AF patches were fragments of one AF scaffold, they differed from the scaffolds only in size and the way they were cultured. Due to the snail-like structure of the AF scaffold, these could be cultured in an upright position. However, an AF patch had to be placed with one side facing down towards the plastic well in which it was cultured.

Cell culture

Human bone marrow aspirates were collected from the vertebral bodies of trauma patients (donor characteristics and cell passages are summarized in Table 1). All patients provided written consent, and the procedure was approved by the ethics committee of the Canton of Bern (with either of the two valid ethical permissions: either SwissEthics #2019-00097, or the general consent of the Insel University Hospital, respectively). The MSCs were then extracted using Histopaque-1077 (Sigma-Aldrich, Buchs, Switzerland; #10771) and expanded in α-minimal essential medium (α-MEM; Gibco, Life Technologies, Zug, Switzerland; #12000063) enriched with 2.2 g/L sodium hydrogen carbonate ($NaHCO_3$; Sigma-Aldrich; #31437), 10 % fetal bovine serum (FBS; Capricorn scientific, Ebsdorfergrund, Germany; #FBS-11A), 1 % penicillin/streptomycin (Sigma-Aldrich; penicillin: #5161, streptomycin: #5711), 1 % HEPES buffer (Thermo Fisher Scientific, Waltham, MA, USA; #15630-056) and 2.5 ng/mL fibroblast growth factor 2 (FGF2; PeproTech; #100-18B-100UG). The cells were passaged once they reached a confluency of 80-90 %. As soon as enough MCSs were available, they were seeded onto the silk scaffolds. To ensure that the cells exclusively attach to the silk, the plastic surfaces on which the scaffolds were placed were pre-coated with 2 % agarose (Sigma-Aldrich; #A9539-100G). The number of cells to be seeded per scaffold was calculated based on the cell densities found in healthy IVDs, which average 4,000 cells/mm^3 in human NP tissue and 9,000 cells/mm^3 in human AF tissue (Maroudas *et al.*, 1975). However, to allow further cell divisions during the culture period on the scaffold, only a third of the physiological cell density was taken, resulting in 1,333 cells/mm^3 for the NP scaffolds and 3,000 cells/mm^3 for the AF samples. Taking the scaffolds' volume and the above mentioned cell densities into account, the following cell numbers were used for seeding: 710,000 for the NP scaffolds, 310,000 for the AF patches, and 20 million cells for the AF scaffolds. After the MSCs had been pipetted evenly onto the scaffolds, the cells were given the chance to acclimatize to their new environment. For this reason, they were first cultured for three days in low-glucose (1 g/L) Dulbecco's Modified Eagle Medium (LG-DMEM; Gibco; #31600083) with added 2.2 g/L $NaHCO_3$, 1 % penicillin/streptomycin, 1 % HEPES buffer, and 10 % FBS. Once this three-day acclimatization period was over, day 0 control samples of each scaffold/patch were isolated. For the remaining samples, the medium was exchanged for chondrogenic inductive medium, which consisted of the same ingredients as the enriched LG-DMEM used for acclimatization, but the FBS was omitted and replaced with 1 % ITS+ (Insulin, transferrin, selenium, bovine serum albumin and linoleic acid; Sigma-Aldrich; #I2521), 1 % non-essential amino acids (Gibco; #11140-035), 172 μM L-ascorbic-acid 2 phosphate (Sigma-Aldrich; #A8960), 100 nM dexamethasone (Sigma-Aldrich; #D4902-25MG), and 10 ng/mL TGF-β1 (PeproTech; #100-21C). On day 7 and 14, only NP scaffolds and AF patches were isolated for further

downstream analysis and then on day 21, samples from all conditions were collected (Fig. 2). All samples were cultured at 37 °C with 20 % O_2 and 5 % CO_2, and the medium was changed twice a week.

Table 1. Donor characteristics, including the gender and age at the time of cell extraction, as well as the passage number with which the cells were seeded onto the silk scaffolds. Abbreviations: AF: annulus fibrosus, NP: nucleus pulposus.

N°	Gender	Age [years]	Passage
1	Male	66	3 (NP scaffolds), 4 (AF scaffolds)
2	Female	19	4
3	Female	69	5 (NP scaffolds), 3 (AF scaffolds)
4	Female	75	3
5	Male	34	3
Mean	N/A	52.6	N/A

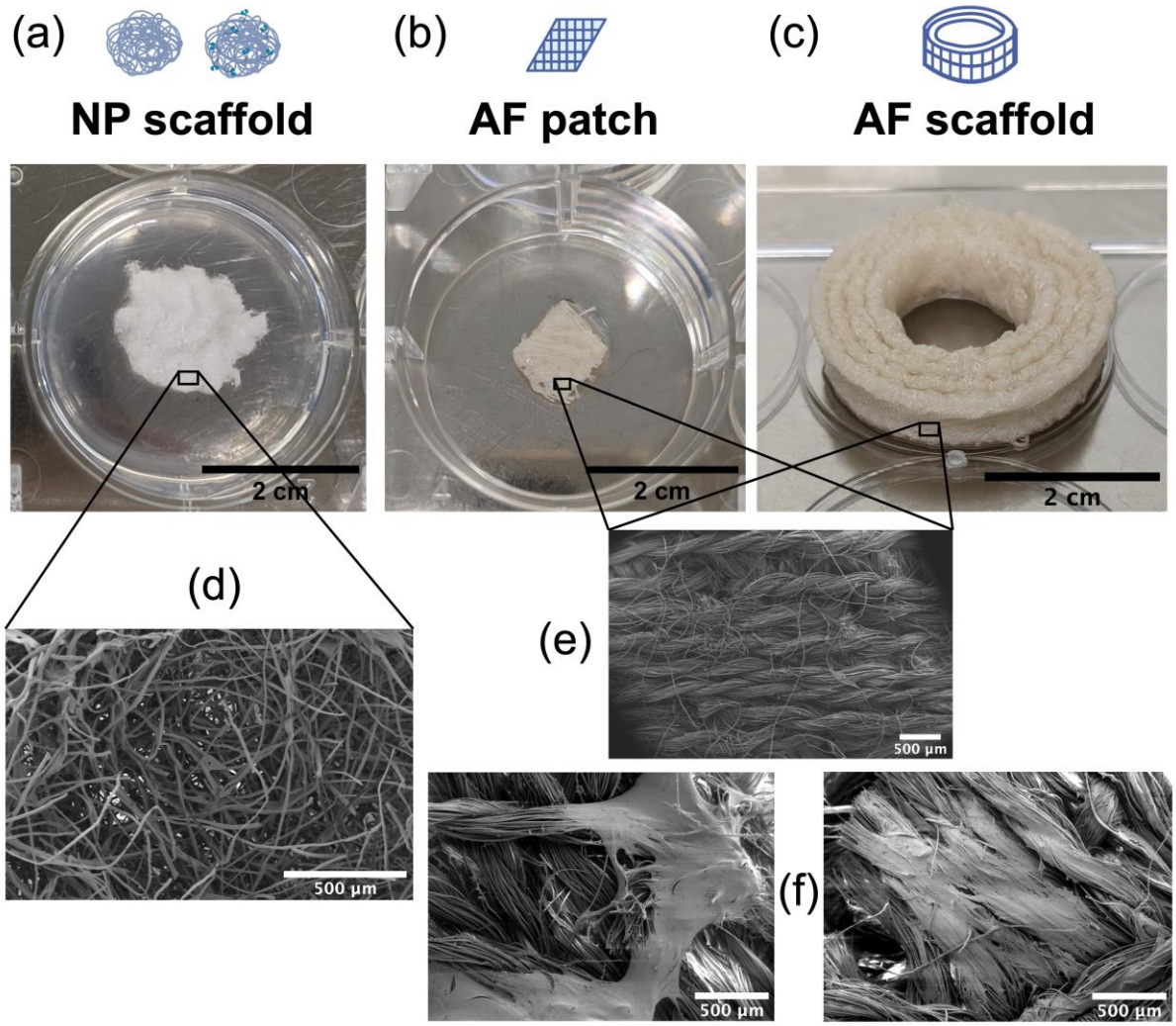

Fig. 1. Macroscopic and scanning electron microscope (SEM) imaging of the silk samples. Macroscopic pictures of the (**a**) NP scaffolds, (**b**) AF patch, and (**c**) AF scaffold, scale bar = 2 cm. (**d**) SEM image of a plain NP scaffold, (**e**) SEM image of a plain AF patch/scaffold, (**f**) SEM images of an AF patch/scaffold with human mesenchymal stromal cells (MSC), scale bar = 500 µm.

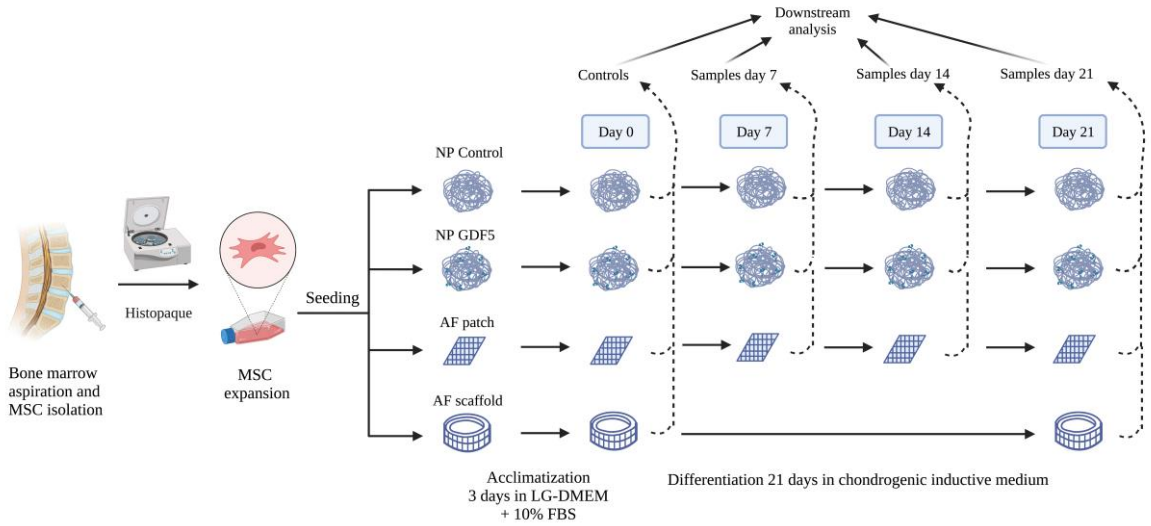

Fig. 2. Overview of the experimental design. MSCs from bone marrow aspirates were isolated and expanded *in vitro* and then seeded onto the different scaffolds. After three days of acclimatization, they were collected as controls or cultivated for an additional either 7, 14 or 21 days in chondrogenic inductive medium.

Metabolic activity and sample digestion

To measure the metabolic activity, a whole AF patch, half of a NP scaffold and approximately ⅒ of an AF scaffold were immersed into 50 µM resazurin sodium salt (Sigma-Aldrich; #R7017-1G) dissolved in FBS-free LG-DMEM (1 mL per AF patch and 2 mL per NP and AF scaffold piece). Then, all samples were incubated at 37 °C. After 60 minutes, the fluorescence was measured at 544 nm excitation and 590 nm emission using an ELISA reader (Spectramax M5, Bucher Biotec, Basel, Switzerland). The relative fluorescence unit (RFU) was normalized to the amount of DNA per sample.

As soon as the RFU was measured, the patches and scaffolds were washed and put into 1 mL or 2 mL papain solution respectively, which was composed of 3.9 U/mL papain (Sigma-Aldrich; #P-3125) and 5 mM L-cysteine hydrochloride (Sigma-Aldrich; #1161509). The samples were then digested over night at 60 °C and on the following day, the remaining residues were removed by centrifugation at 13,000 RPM for eight minutes. These samples were then used to determine the DNA, glycosaminoglycan (GAG), and hydroxyproline (HYP) content.

DNA content

The DNA was measured using Quant-iT™ PicoGreen® dsDNA reagent (Thermo Fisher Scientific; #P7589). Therefore, samples were mixed 1:1 with the diluted PicoGreen® and incubated for four minutes. Once incubated, the fluorescence was measured at 487 nm excitation and 525 nm emission.

Glycosaminoglycan content

The amount of GAG produced in the silk scaffolds was determined using 1,9-dimethyl-methylene blue (Sigma-Aldrich; #341088). Thus, the absorbance was measured at a wavelength of 600 nm and the results were extrapolated using a standard curve based on chondroitin sulphate (Sigma-Aldrich; #C6737).

Hydroxyproline content

A HYP assay was performed to estimate the amount of collagen produced by the cells since mammalian collagen comprises approximately 13.5 % HYP. Therefore, the digested samples were mixed 1:1 with 12M HCL (Sigma-Aldrich; #30721) and incubated at 95 °C for 20 hours. On the following day, the samples were neutralized with 10M NaOH (Sigma-Aldrich; #71690) and blended with a 1:1 charcoal/resin mix (Sigma-

Aldrich; #05105 / Bio-Rad Laboratories, Cressier, Switzerland; #143-7425). After centrifugation, the supernatant was mixed with saturated NaCl (Sigma-Aldrich; #71380) and Chloramin T (Sigma-Aldrich; #31224). Then, the samples and standard were mixed with 4-Dimethylamino-Benzaldehyd (DABA; Sigma-Aldrich, #39070). After 15 minutes of incubation at 60 °C, the samples' absorption was measured at 560 nm and compared to a standard made of L-4-Hydroxy-Proline (Sigma-Aldrich; #56250).

Gene expression

One whole AF patch, half of a NP scaffold and approximately ⅒ of an AF scaffold per condition were immersed into lysis buffer (Sigma-Aldrich; #L8285-70ML) containing 2-mercaptoethanol (Sigma-Aldrich; M3148-9ML). The RNA was extracted using the GenElute™ Mammalian Total RNA Miniprep kit (Sigma-Aldrich; #RTN70-1KT) and genomic DNA was digested using on column DNase I (Sigma-Aldrich; #DNASE70-1SET). Once

Table 2. Overview of all genes investigated, and the corresponding primers used for qPCR in this study.

Gene type	Full name	Symbol	NCBI gene ID	Forward and reverse primer sequences
Reference gene	Glyceraldehyde-3-Phosphate Dehydrogenase	*GAPDH*	2597	f - AAT CCC ATC ACC ATC TTC CAG r - GAG CCC CAG CCT TCT CCA T
Anabolic markers	Aggrecan	*ACAN*	176	f - CAT CAC TGC AGC TGT CAC r - AGC AGC ACT ACC TCC TTC
	SRY-box transcription factor 9	*SOX9*	6662	f – GAG ACT TCT GAA CGA GAG r - GGC TGG TAC TTG TAA TCC
	Collagen Type 1, Alpha 2 Chain	*COL1*	1278	f - GTG GCA GTG ATG GAA GTG r - CAC CAG TAA GGC CGT TTG
	Collagen Type 2, Alpha 1 Chain	*COL2*	1280	f - AGC AGC AAG AGC AAG GAG AA r - GTA GGA AGG TCA TCT GGA
	Collagen Type 10, Alpha 1 Chain	*COL10*	1300	f - GAA TGC CTG TGT CTG CTT r - TCA TAA TGC TGT TGC CTG TTA
Catabolic markers	ADAM Metallopeptidase with Thrombospondin Type 1 Motif 4	*ADAMTS4*	9507	f - TTC CTG GAC AAT GGC TAT GG r - GTG GAC AAT GGC GTG AGT
	Matrix Metallopeptidase 13	*MMP13*	4322	f - AGT GGT GGT GAT GAA GAT r - CTA AGG TGT TAT CGT CAA GTT
Nucleus pulposus markers	Cluster of Differentiation 24	*CD24*	100133941	f - GCT CCT ACC CAC GCA GAT TTA r - GCC TTG GTG GTG GCA TTA GT
	Cytokeratin 8	*KRT8*	3856	f - CCA GGA GAA GGA GCA GAT r - CGC CTA AGG TTG TTG ATG TA
	Cytokeratin 19	*KRT19*	3880	f - TAT GAG GTC ATG GCC GAG CA r - GGT TCA ATT CTT CAG TCC GGC
Annulus fibrosus markers	Cluster of Differentiation 146	*CD146*	4162	f - GGA GCC TGA GGA GGT CGC TA r - ACT CCA CAG TCT GGG ACG AC
	Integrin Binding Sialoprotein	*IBSP*	3381	f - AGG GCA GTA GTG ACT CAT CCG r - AGC CCA GTG TTG TAG CAG AAA G
	Fibulin 1	*FBLN1*	2192	f - TCT CTG TGG ATG GCA GGT CA r - ACA CTG GTA GGA GCC GTA GA

the RNA was extracted, cDNA was synthesized using the High-Capacity cDNA kit (Thermo Fisher Scientific; #4368814) with a MyCycler™ Thermal Cycler system (Bio-Rad; #1709703). For the subsequent quantitative polymerase chain reaction (qPCR), the cDNA was mixed with the primers of interest (Table 2) and with iTaq Universal SYBR Green Supermix (Bio-Rad; #1725122). Finally, the qPCR was performed using a CFX96™ Real-Time System (Bio-Rad; #185-5096) and the relative gene expression was determined with the $2^{-\Delta\Delta Ct}$ method while using *GAPDH* as a reference gene (Livak and Schmittgen, 2001). All gene expressions were calculated relative to the day 0 value within the same group, except for the NP GDF5 group where the gene expression was calculated relative to day 0 of the NP Control group to observe the direct influence of GDF5.

Imaging

Histology

The silk scaffolds and patches were first fixed for 48 hours in 4 % formalin (VWR, Radnor, USA; #9713-9010). After fixation, the formalin was rinsed out and in a next step all samples were dehydrated, embedded into paraffin, and then cut into 15 μm thin sections (Microm HM355; Thermo Fisher Scientific). Once mounted onto polysine adhesion slides (Thermo Fisher Scientific; #J2800AMNZ), the samples were dried overnight and then stained with Alcian blue (Sigma-Aldrich; #A5268-10G). Closeup images were taken using a Nikon Eclipse E800 (Nikon, Minato, Japan).

Scanning electron microscopy

250,000 MSCs were seeded onto an AF patch and cultured for 24 hours in LG-DMEM-based expansion medium supplemented with 10 % FBS. On the following day, the expansion medium was replaced with chondrogenic inductive medium and the cells were cultured for another week. Both the expansion- and the chondrogenic inductive medium were the same used for the main study. After one week, the AF patches and plain NP scaffolds were washed with PBS and fixed with 2.5 % glutaraldehyde for one hour. Then, the samples were washed with 0.1 M cacodylate buffer and postfixed with 1 % OsO_4. In a next step, critical point drying was applied (Leica EM CPD300; Leica Microsystems, Heerbrugg, Switzerland) and then 10 nm platinum was sputtered onto the samples (BalTec SCD004; Leica Microsystems). Finally, images were taken with a digital field emission scanning electron microscope (SEM; DSM 982 Gemini; Carl Zeiss, Jena, Germany) at an accelerating voltage of 4.2-5 kV and a working distance of 6.7-11 mm.

Statistical analysis

Up to five biological replicates/human cell donors (*N*) and between 1 and 3 technical replicates (n) were used for each experiment. The exact number of replicates is given in the respective figure's legend. Data are presented as mean ± standard deviation (*SD*), except for the gene expression, which is presented as mean + *SD*, and the GDF5 release profile, which is presented as mean of the technical replicates. For comparisons within a group, a Kruskal-Wallis test with Dunn correction was applied for the NP scaffolds and AF patches and a Mann-Whitney U test for the AF scaffolds. For inter-group comparisons, an unpaired and unmatched two-way ANOVA was used for multiple comparison and corrected by a Tukey multiple comparison test. A *p*-value less than 0.05 was considered statistically significant. All statistical tests were carried out using GraphPad Prism (Version 9.5.1 for macOS, GraphPad Software, San Diego, California, USA).

Results

GDF5 release profile

The standard curve demonstrated reactivity and accuracy and a detection limit of 6.7 pg/mL of GDF5 could theoretically be detected (Fig. 3**a**). No GDF5 was detected in the solutions that were incubated with the NP Control scaffold (Fig. 3**b**). In addition, the solutions that were incubated with the GDF5-functinalized NP scaffold contained no detectable GDF5 (Fig. 3**b**). Therefore, all the GDF5 that was coupled onto the scaffold remained on the scaffold during the entire culture period and thus was available for signalling.

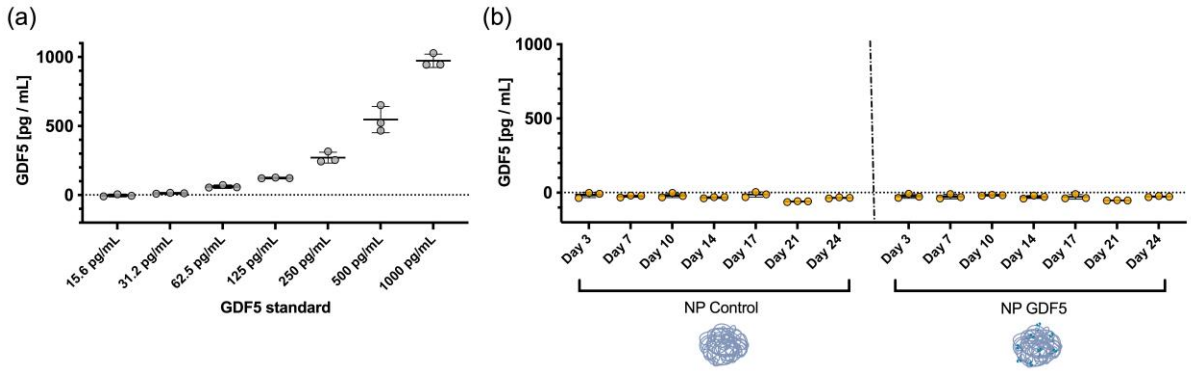

Fig. 3. GDF5 release profile. (**a**) Standard curve of predefined GDF5 concentrations. (**b**) Measured GDF5 in NP Control and NP GDF5 scaffolds. Mean ± *SD*, n = 3.

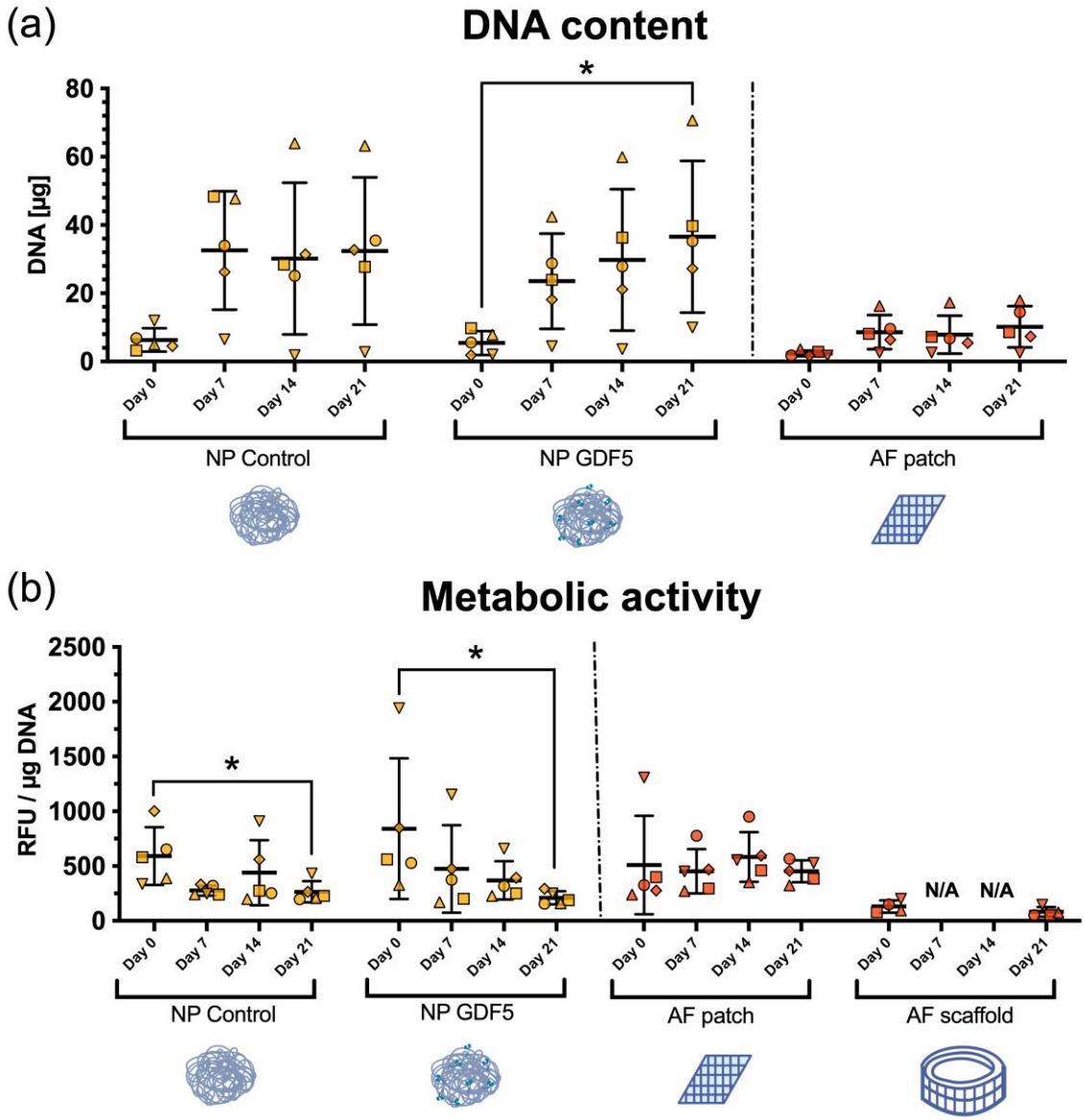

Fig. 4. DNA content and metabolic activity. (**a**) DNA content of NP scaffolds and AF patches at different time points. (**b**) Metabolic activity of all tested silk samples at different time points. The values are represented as relative fluorescent units (RFU) normalized to the amount of DNA per sample. Mean ± SD, N = 4-5, n = 2 concerning the DNA and n = 1 concerning the metabolic activity, *p*-value: * < 0.05.

DNA content and metabolic activity

On day 0, the donors within each individual condition showed a comparable amount of DNA. During the 21-day culture period, the amount of DNA generally increased in all conditions, however, only in the GDF5 NP scaffolds a significant ($p < 0.05$) increase was recorded, where a five-fold augmentation was observed compared to day 0 (Fig. 4**a**). Furthermore, a strong trend ($p = 0.062$) towards increasing DNA could be seen in the AF patches. Regarding the metabolic activity of the cells, the highest values were observed in the NP scaffolds on day 0, but then significantly ($p < 0.05$) decreased after 21 days (Fig. 4**b**). Notably, no significant changes in cell activity were found for the AF scaffolds and patches.

Gene expression

Anabolic genes

The anabolic genes were generally upregulated throughout the culture period. *ACAN*, for example, steadily increased in all conditions and displayed a significant ($p < 0.05$) upregulation in the NP GDF5 group (254 ± 265.2-fold increase) and in the AF scaffolds (21 ± 19.4-fold increase) after 21 days (Fig. 5**a**). SRY transcription factor 9 (*SOX9*) remained unchanged regardless of the culture duration and the silk scaffold tested (Fig. 5**b**). *COL1* only showed significant changes in the AF groups and not in the NP scaffolds (Fig. 5**c**). Here, a significant upregulation was seen in the AF patch on day 7 ($p < 0.05$) and day 14 ($p < 0.05$) and a strong trend on day 21 ($p = 0.08$). Moreover, *COL1* was also significantly ($p < 0.05$) upregulated in the AF scaffold after 21 days. Next, *COL2* showed a similar, but much more prominent pattern than *ACAN* (Fig. 5**d**). *COL2* was significantly higher expressed in all groups at the end of the culture ($p < 0.05$ for the AF scaffold, $p < 0.01$ for the rest). However, the NP scaffolds showed an almost ten times higher upregulation of *COL2* than the AF samples. Again, the highest expression was found in the NP GDF5 scaffolds (1.2 million ± 1.28 million-fold increase). Finally, *collagen type 10* (*COL10*) gradually increased during the culture period and was already significantly ($p < 0.05$) upregulated in the NP Control group and in the AF patches after 14 days and eventually in all groups after 21 days ($p < 0.05$ for the AF scaffold, $p < 0.01$ for the rest) (Fig. 5**e**).

Catabolic genes

The catabolic marker *A disintegrin and metalloproteinase with thrombospondin motifs 4* (*ADAMTS4*) was usually highest at the beginning of the culture but then gradually decreased towards the end (Fig. 5**f**). At day 7, *ADAMTS4* was significantly upregulated in the AF patches but not anymore at day 14 and day 21. In addition, *ADAMTS4* was significantly downregulated in the NP GDF5 scaffolds on day 21 compared to day 7. The collagenase *Matrix Metallopeptidase 13* (*MMP13*) was only found to be significantly upregulated in the AF samples (Fig. 5**g**). Here, the AF patch showed a significant upregulation after seven days and the AF scaffold after 21 days ($p < 0.05$). Furthermore, *MMP13* was significantly ($p < 0.001$) higher in the AF scaffold on day 21 than the other conditions on the same day.

Nucleus pulposus markers

CD24 was significantly ($p < 0.05$) upregulated in the NP scaffolds and AF patches after 14 days of culture with chondrogenic inductive medium and it stayed at a high level for the remaining time (ranging between 305-fold and 566-fold upregulation) (Fig. 6**a**). Notably, however, in the NP GDF5 scaffolds it was already significantly ($p < 0.05$) upregulated after 7 days. *KRT8* remained unchanged in the NP scaffolds but was significantly downregulated in the AF patches on day 14 (Fig. 6**b**). The final NP marker, *KRT19*, decreased continuously in the NP scaffolds and the AF patch (Fig. 6**c**). The lowest point was reached at day 21 where the expression of *KRT19* was significantly ($p < 0.05$ for NP Control and $p < 0.01$ for NP GDF5 and the AF patch) lower and approximately ten times less compared to day 0.

Annulus fibrosus markers

CD146 was significantly ($p < 0.05$) upregulated in both the AF patches and AF scaffolds at every time point tested (Fig. 6**d**). Moreover, *CD146* was also significantly ($p < 0.05$) upregulated in the NP scaffolds, however, only until day 14 in the NP Control samples and only on day 7 in the NP GDF5 samples. Next, *IBSP* was exclusively significantly ($p < 0.05$) higher expressed in the AF patches when comparing day 7 with day 21 (Fig. 6**e**). No significant differences were observed in the NP scaffolds. Finally, although *FBLN1* did not significantly change during a culture period of 21

days, it tended to be more downregulated in the NP scaffolds than in the AF samples (Fig. 6**f**).

Extracellular matrix production

The GAG content, which was normalized to the amount of DNA, stayed relatively constant over the culture period without any significant changes (Fig. 7**a**). Only the AF scaffolds showed a trend (p = 0.11) of increased GAG at day 21. Comparable results were also found with the amount of HYP per DNA, where no differences could be detected between the different time points in all groups (Fig. 7**b**). Finally, the ratio between GAG and HYP was estimated to determine the tissue specific differentiation towards NP-like tissue. Here, a significant (p < 0.05) increase in the ratio was seen in the NP GDF5 scaffolds from day 7 to day 21 and the highest value was found in the NP Control scaffold on day 21 (4.6 ± 3.6) (Fig. 7**c**).

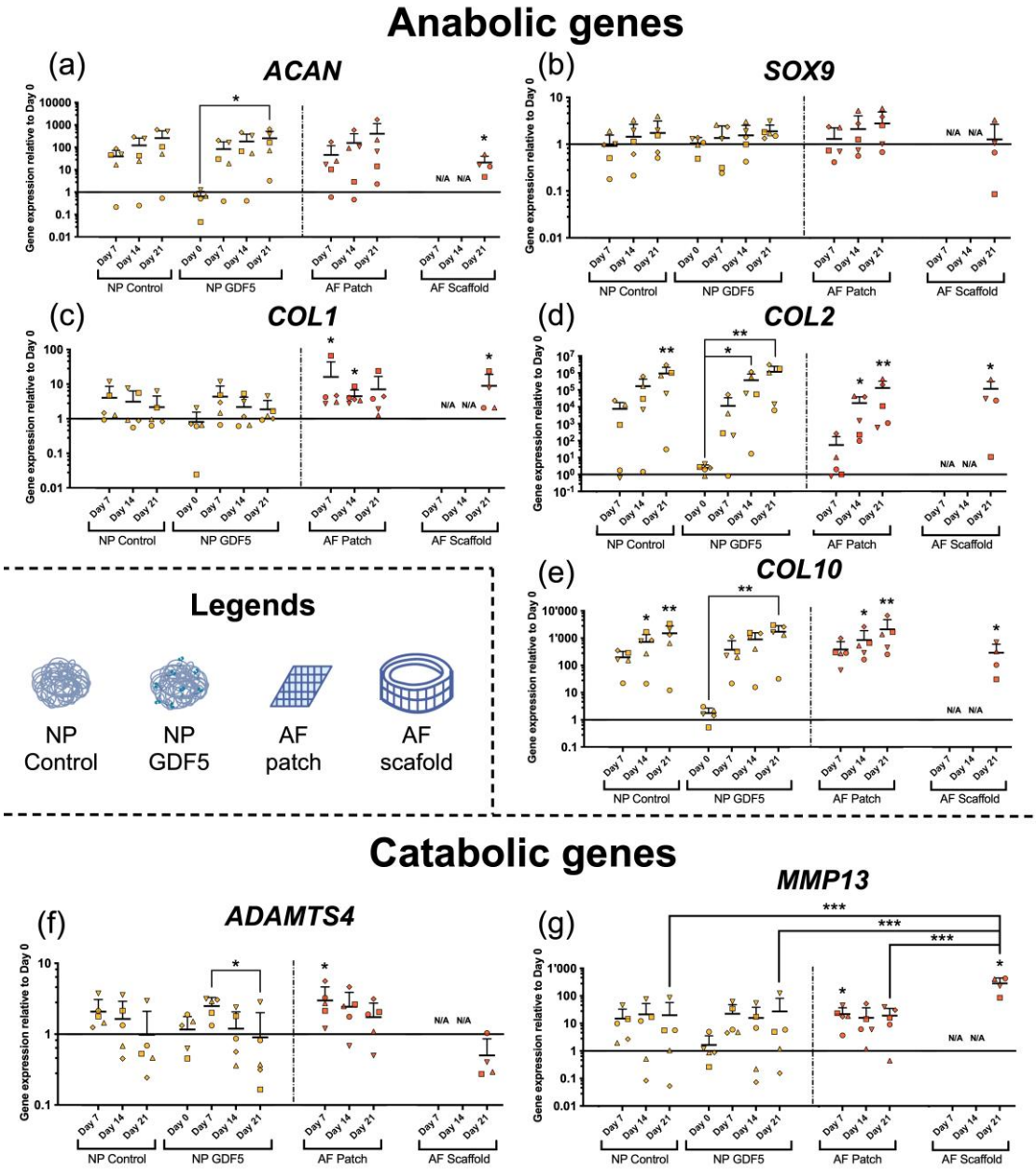

Fig. 5. Relative gene expression of anabolic and catabolic markers. Anabolic genes, including (**a**) ACAN, (**b**) SOX9, (**c**) COL1, (**d**) COL2, and (**e**) COL10; and catabolic genes, including (**f**) ADAMTS4 and (**g**) MMP13. Mean + SD, N = 4-5, n = 2, p-value: * < 0.05, ** < 0.01, *** < 0.001.

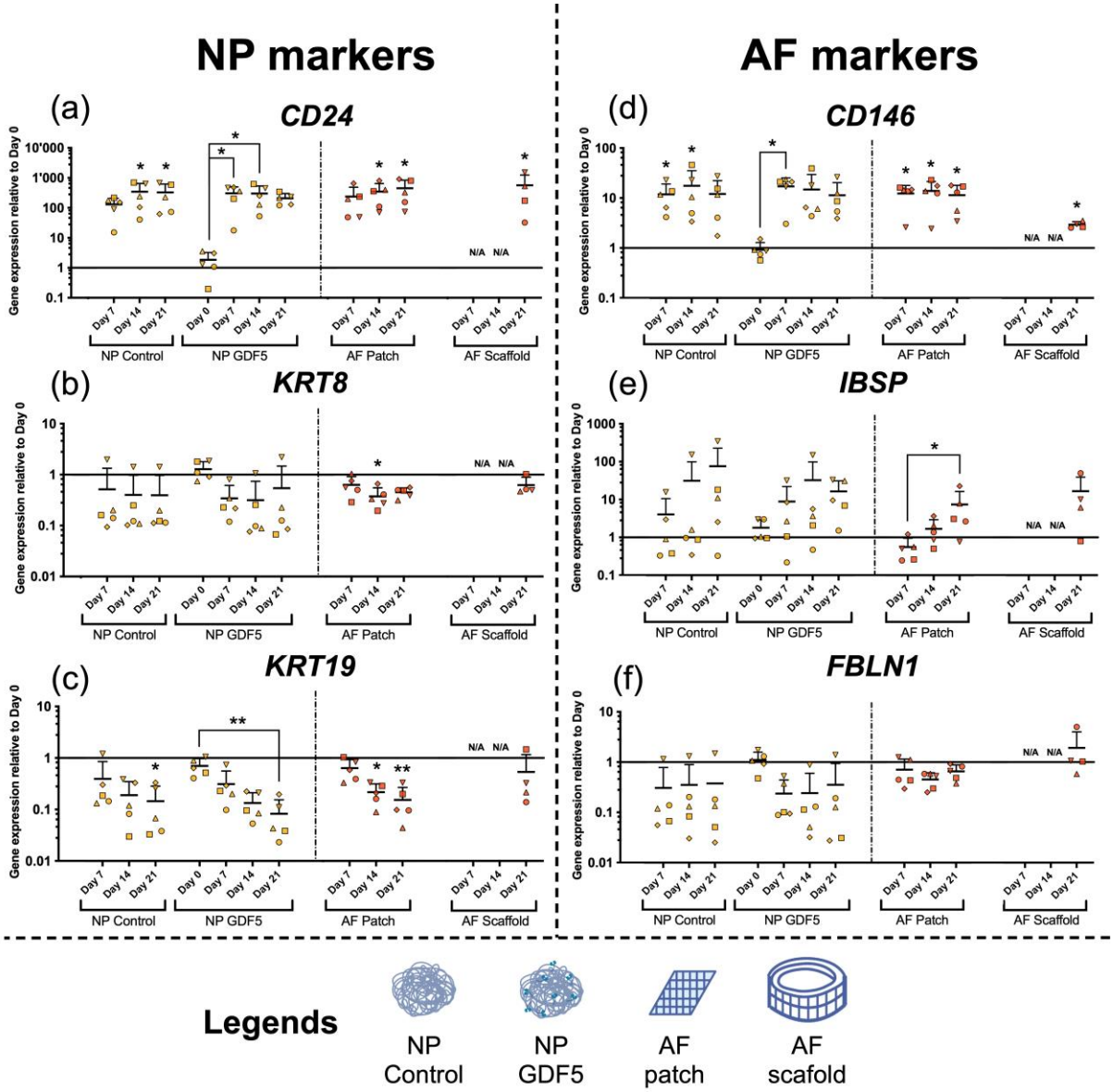

Fig. 6. Relative gene expression of intervertebral disc markers. Nucleus pulposus (NP) markers, including (**a**) *CD24*, (**b**) *KRT8*, and (**c**) *KRT19*; and annulus fibrosus (AF) markers, including (**d**) *CD146*, (**e**) *IBSP*, and (**f**) *FBLN1*. Mean + *SD*, *N* = 4-5, n = 2, *p*-value: * < 0.05, ** < 0.01.

Imaging

The images taken by the SEM revealed the isotropic fibre network with interconnected pores of the NP scaffolds (Fig. 1**d**) and the mesh-like structure with alternating orientation of the silk yarns in the AF constructs (Fig. 1**e**). Furthermore, the images also showed how the MSCs spread over the silk and how they tightly entangled the silk yarns (Fig. 1**f**).

To visualize the sulphated GAG within the silk, they were stained with Alcian blue. In the NP scaffolds, a considerable increase in the intensity of the stain could be seen from day 0 to day 21 (Fig. 8**a-d**). Moreover, a notable difference was observed between the NP GDF5 and the NP Control scaffold on day 21, indicating a higher amount of GAG in the NP GDF5 scaffolds (Fig. 8**b,d**). A similar tendency was visible for the AF scaffold and AF patches but much less prominent compared to the NP scaffolds (Fig. 8**e-h**).

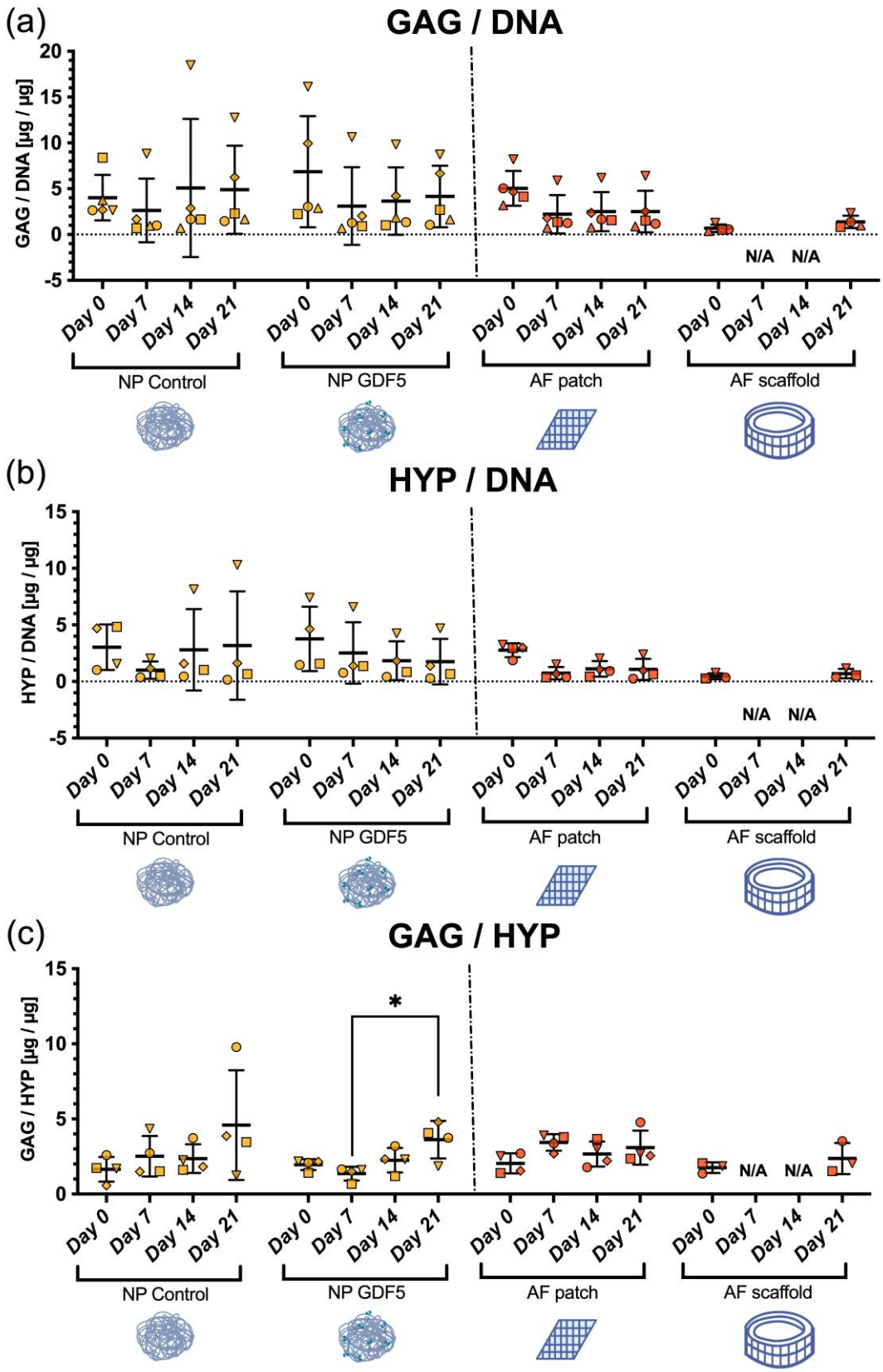

Fig. 7. Extracellular matrix production. (**a**) Glycosaminoglycan (GAG) content in the silk relative to the DNA content. (**b**) Hydroxyproline (HYP) content in the silk relative to the DNA content. (**c**) Amount of GAG relative to the amount of HYP. Mean ± *SD*, *N* = 3-5, n = 3 concerning the GAG and n = 2 concerning the HYP, *p*-value: * < 0.05.

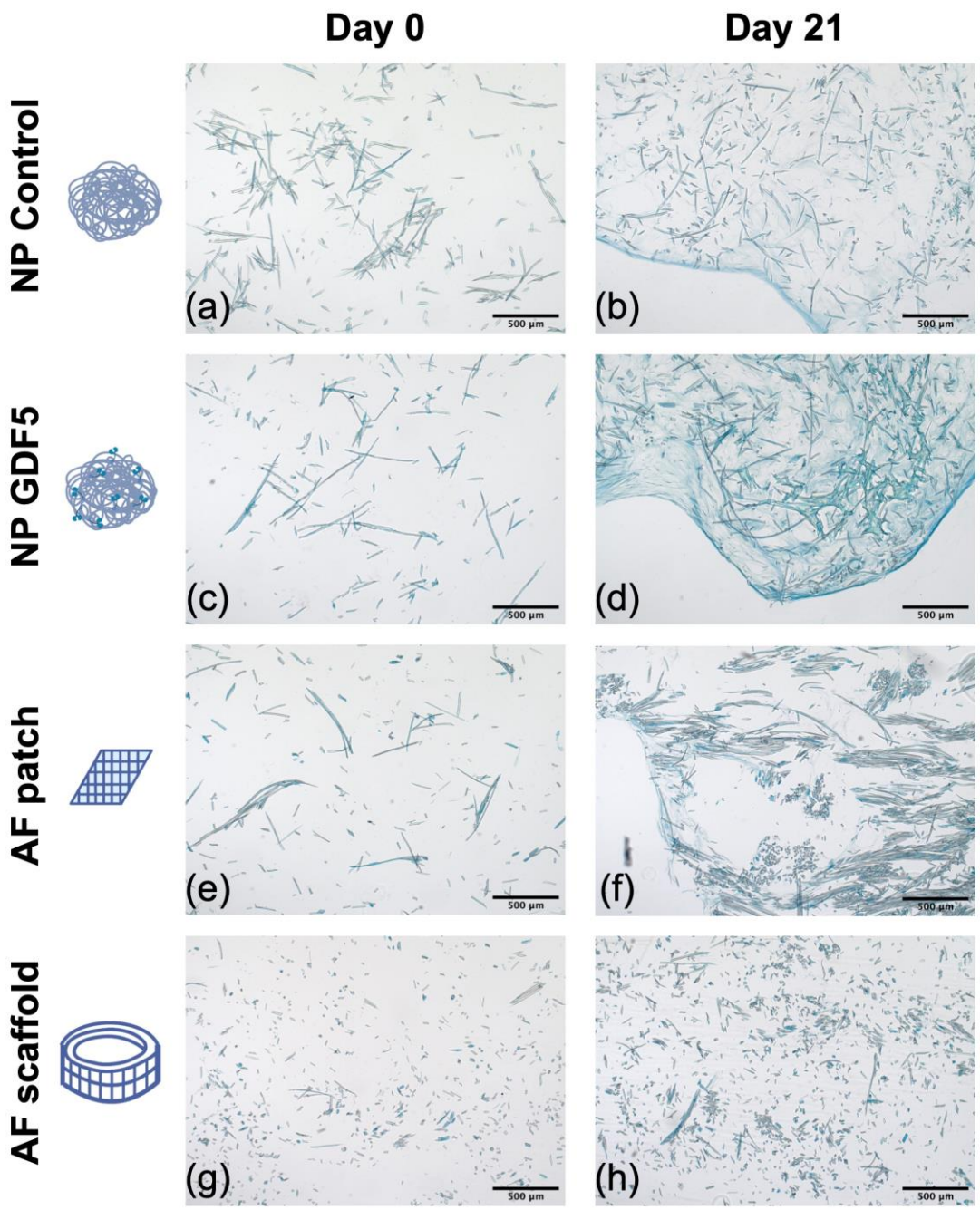

Fig. 8. Alcian blue staining of the silk samples. (**a**), (**b**) NP Control scaffold, (**c**), (**d**) NP GDF5 scaffold, (**e**), (**f**) AF patch, and (**g**), (**h**) AF scaffold seeded with human mesenchymal stromal cells (MSC) on day 0 and on day 21. Scale bar = 500 µm.

Discussion

In the present study, we aimed to create NP- and AF-like tissue made of novel silk scaffolds and human MSCs with a size and cell density similar to what can be found in a healthy human IVD. Regarding the cell density, the MSCs were originally seeded with one third of the average number found in a healthy adult IVD (Maroudas *et al.*, 1975). At day 0, three days after the cells were seeded onto the silk scaffolds, all donors within the same group displayed a very similar DNA content, which indicated that seeding of the different donors was performed uniformly. From day 7 onwards, however, the donor variability increased notably. For the majority of the donors, the DNA content increased by a factor 4-5. However, there was one donor whose DNA

content did not increase at all and another donor's DNA increased by a factor 6 by the end of the culture period. Nevertheless, the amount of DNA increased on average by a factor 4-5, instead of the anticipated 3-fold increase that would have led to a physiological value. However, when taking into account that probably not all cells survived the transfer process onto the silk and presumably a certain number of cells did not attach to the scaffolds, a 4-5-fold increase in the initial cell density seems appropriate. Now regarding the MSCs' metabolic activity, it started with a relative high value and then in the case of the NP scaffolds gradually decreased during the experiment. Despite this, the cells remained very much alive and proliferated, as shown by the DNA content. From this we conclude that the cells were able to adapt on the NP scaffolds but were probably metabolically more active during the expansion on plastic. Furthermore, the majority of the changes happened during the first week of culture with chondrogenic inductive medium. After the first week, the cell proliferation as well as the metabolic activity seemed to have reached a "steady state" in which the cells noticeably slowed down their proliferation rate, but also stabilized their metabolic activity until the end of the culture. Interestingly, this gradual decrease of the metabolic activity was not found with the AF samples. Here, the activity stayed very stable throughout the culture period. This is in accordance with the results of See et al., where the metabolic activity of rabbit MSCs on a silk scaffold mimicking the lamellae of an AF remained unchanged for four weeks (See *et al.*, 2011).

One of the aims of this study was to evaluate if human MSCs can be guided towards an NP- and/or AF-like phenotype based on the morphology of the silk scaffold itself and whether functionalization with GDF5 would further enhance the cellular phenotype. First of all, we can deduct from the gene expression profile that the cells overall displayed a highly anabolic phenotype. All anabolic markers except for *SOX9* were significantly upregulated at multiple occasions during the 21-day culture period with chondrogenic inductive medium. In particular, the extent of *COL2* upregulation came as a surprise, since in comparable studies, in which MSCs were also cultured in a 3D environment with a similar chondrogenic inductive medium, *COL2* upregulation was observed in the 10- to 100-folds rather than in the 100,000-folds as in our study (Clarke *et al.*, 2014; Frauchiger *et al.*, 2018a; Salonius *et al.*, 2020). The effect of this anabolic gene expression profile was also well visible on the NP scaffolds stained with Alcian blue. Especially the addition of GDF5 enhanced the production of sulphated GAG in the scaffold, as the Alcian blue stain was more intense than with TGF-β1 alone. What further underlined the anabolic phenotype was the significant downregulation of the catabolic marker *ADAMTS4*, which peaked at day 7 but then gradually declined to baseline levels. The only incidence of increased catabolic gene expression at day 21 was found for *MMP13* in the AF scaffolds, where it was significantly higher expressed than all other conditions. Another gene that was also significantly upregulated in all samples was *COL10*. *COL10* is often overexpressed in MSC culture with chondrogenic inductive medium containing TGF-β and unfortunately, our experiments are no exception here (Mueller *et al.*, 2010; Pelttari *et al.*, 2006). A high *COL10* expression usually indicates that the cells have a hypertrophic phenotype in the chondrogenic lineage and are heading towards an osteogenic transition and apoptosis (Hallett *et al.*, 2021). Nevertheless, the strong anabolic phenotype of our silk samples is promising as it represents healthy tissue.

Now regarding the IVD tissue specific differentiation, some interesting differences were discovered between the NP scaffolds and the AF samples. On the one hand, *COL1* was only significantly upregulated in the AF samples and not in the NP scaffolds. On the other hand, the expression of *COL2* was almost ten times higher in the NP scaffolds than in the AF samples and the highest expression was found in the GDF5-funcitonalized group. Moreover, although *ACAN* was also significantly upregulated in the AF scaffolds by day 21, the gene was more than ten times higher expressed in the GDF5-functionalized NP scaffolds. As a matter of fact, human NP tissue is rich in proteoglycans like ACAN and out of all collagens, COL2 is the one that predominates, whereas in the outer AF tissue, COL1 predominates and the proteoglycan

content is also lower than in the NP (Adams *et al.*, 1977; Iatridis *et al.*, 2007). Therefore, based on these results, we concluded that our NP scaffolds, particularly the GDF5-functionalized scaffolds, displayed more characteristics of native NP tissue, while the AF samples showed more characteristics of AF tissue.

Although the tissues' expression of certain collagens and proteoglycans indicated some typical characteristics that can be found in NP and AF tissue, other NP- and AF-specific markers only partially confirmed these findings. *CD24*, a molecular marker to distinguish NP cells from other cell types, was upregulated in all conditions. Thus, it confirmed the NP-like characteristics of the NP scaffolds, it also revealed some NP-like features on the AF samples. The other NP markers *KRT8* and *KRT19* were either unchanged or significantly downregulated and failed to verify the NP-like characteristics of the NP scaffolds proposed by the anabolic markers and *CD24*. Notably, when Clarke *et al.* (2014) worked with bone marrow MSCs, they were also unsuccessful to enhance the expression of *KRT8* and *KRT19* with GDF5-enriched culture medium, but managed to significantly upregulate these genes when adipose MSCs were used instead. A significant upregulation of these NP-specific markers with bone marrow MSCs could only be achieved when GDF5 was exchanged for growth differentiation factor 6 (GDF6). Interestingly, Frauchiger *et al.* (2018a) also used GDF6 to differentiate bone marrow MSCs towards an IVD-like phenotype. Similar to our study, their MSCs were cultured on silk patches. After 21 days, they also found an upregulation of anabolic markers, however, in contrast to Clarke et al., *KRT8* and *KRT19* were generally downregulated. Strikingly, the positive impact of TGF-β1 combined with GDF5 that we previously found in the anabolic markers was absent in the NP-specific markers. The idea of combining these two growth factors to further improve NP-like cell differentiation was originally realized by (Colombier *et al.*, 2016). TGF-β1 or GDF5 alone already had some notable effects on the differentiation potential of adipose MSCs, however, the full potential was reached when both growth factors were combined, as this resulted in a significantly higher expression of anabolic genes and NP markers. Although we were able to confirm some anabolic benefits when GDF5 was added to TGF-β1, the effects were substantially more mellow to what Colombier *et al.* (2016) reported and it did not significantly upregulate NP-specific markers compared to TGF-β1 alone. The AF markers revealed a somewhat clearer picture than the NP-specific markers. For example, *CD146* was already significantly higher expressed in the AF samples on day 7 and stayed significantly upregulated until the end of the culture period. In contrast, *CD146* remained significantly upregulated in the NP Control scaffolds for 14 days and in in the NP GDF5 scaffolds only for the first week. Consequently, based on the expression of *CD146*, the AF-like characteristics persisted longer in the AF samples than in the NP scaffolds. Moreover, *IBSP*, a second marker used to distinguish AF-like cells from NP-like cells, was significantly upregulated exclusively in the AF patches. The only AF marker that showed no significant changes was *FBLN1*. However, *FBLN1* tended to be more downregulated in the NP samples than the AF samples. Therefore, with the *COL1* expression in mind, we concluded that the MSCs managed to differentiate into chondrogenic cells with some AF-like characteristics.

In contrast to the relatively high expression of *ACAN* and the histological findings, the actual tissue matrix production proved to be rather low in our study. In a comparable study, the GAG/DNA gradually increased and ranged between 10-25 (μg/μg) after 21 days of culture (Frauchiger *et al.*, 2018a). The same low trend could also be observed when the amount of HYP was measured and normalized to the DNA content. Since the HYP content correlates with the amount of collagen, the here found results are in direct contradiction to the *COL1* and especially to the very high *COL2* expression found in all conditions. An explanation why the measured ECM production did not match with the results found in the qPCR data and the histology could be that potentially only a fraction of the synthesized GAG and collagen was extracted after the overnight papain digestion of the samples. This would indicate that a large portion of the ECM was still attached to the undigested silk residue, which could not be analysed. However, at least when the GAG was normalized

to the HYP, a clear direction was visible with the NP scaffolds. The GDF5-functionalized scaffolds showed significant increase in the GAG to HYP ratio from day 7 to day 21. The higher the GAG to HYP ratio, the closer the *de novo* formed tissue resembles juvenile NP tissue (Risbud *et al.*, 2015). In fact, the ratio found in the juvenile NP is usually around 27:1 and decreases with age to about 5:1. With that in mind, our NP scaffolds would more closely resemble older NP tissue.

Interestingly, although the AF patches and AF scaffolds generally performed similarly, there were some discrepancies. This included (i) the expression of *MMP13*, which was significantly higher expressed in the AF scaffolds compared to the AF patches, (ii) *ADAMTS4*, which tended to be downregulated in the AF scaffolds but was upregulated in the AF patches, and (iii) a slightly higher metabolic activity in the AF patches than in the AF scaffolds. Even though the AF samples had the same morphological surface structure, the AF scaffolds were wound into a snail-like shape, likely allowing for more cell-cell-contact and consequently more cell-cell-interaction compared to the AF patches. An increased cell-cell-contact is known to cause a stronger mediation of Notch signalling, which plays an essential role in the chondrogenic differentiation of MSCs (Chen *et al.*, 2015). Consequently, changes in cell-cell-contact or -interaction could lead to a different cell behaviour.

In addition to the biological compatibility of the silk scaffolds, there is understandably also the question of how suitable the scaffolds are under mechanical load and how much the mechanical properties resemble those of a native IVD. Therefore, a very recent study by Wöltje *et al.* (2023) tested the tensile strength and stiffness of the exact same AF scaffolds used in this study. In a wet state, the AF scaffolds presented a tensile strength of 12.2 MPa, which is very close to the tensile strength found in a human AF (4 to 10 MPa) (Green *et al.*, 1993; Skaggs *et al.*, 1994). The Young's modulus of the wet AF scaffolds was measured at 317 MPa. As the Young's modulus of human AF is usually within a range of 10 to 40 MPa, the AF scaffolds we used in this study were approximately ten times stiffer than native AF tissue (Acaroglu *et al.*, 1995; Elliott and Setton, 2001; O'Connell *et al.*, 2012; Wagner and Lotz, 2004).

Finally, there are some limitations to this study, which we would like to address. As mentioned earlier, one major problem we faced was to efficiently degrade the silk scaffolds to extract the produced extracellular matrix. Although SF is a protein and is consequently subjected to proteolytic digestion, it is known to be very resilient as it is able to retain its tensile integrity for a long time *in vivo* (> 50 % tensile integrity after 60 days) (Altman *et al.*, 2003). The most efficient enzymes known to degrade SF-films or -sheets are proteinase K and protease XIV (Brown *et al.*, 2015; Li *et al.*, 2003). We tried to digest the scaffolds with proteinase K or protease XIV at concentrations up to 32 U/mL or using our standard papain protocol (3.9 U/mL). However, after one week of incubation with proteinase K, protease XIV, or papain, all samples were poorly digested and differed little from each other. The reason for the impaired digestion was probably that we were working with scaffolds and not with films or fleeces as previously described by Brown *et al.* (2015) and Li *et al.* (2003). Therefore, we assumed that certain contradictions between the GAG/DNA content and the gene expression profile, as well as some discrepancies between the DNA content and the metabolic activity, were due to the inability to properly digest the silk. A possible alternative in future studies could be to analyse certain proteins such as COL1 or COL2 directly on the scaffolds themselves by means of immunofluorescence staining, rather than trying to extract the produced ECM from the scaffolds. Another limitation we faced was that we were unable to display the AF scaffolds' DNA content in a representative way. As we could not measure the DNA of a whole AF scaffold, approximately one tenth of an AF scaffold was actually used for further downstream analysis. However, since one tenth of a scaffold was an approximation, the DNA content would have varied greatly based on the size of the cut. For this reason, we have chosen not to display the AF scaffolds' DNA content at any given time point.

Conclusions

In conclusion, we managed to create tissue with a cell density and size similar to what can be found in a healthy human IVD with some NP-like and AF-like characteristics. The biocompatibility of the silk scaffolds was given because the cells

proliferated throughout the culture period. Furthermore, the tissue-specific morphologies of the silk scaffolds differently influenced the differentiation potential of the cultured MSCs, as the cells on the NP scaffolds exhibited more NP-like characteristics, while the cells on the AF scaffolds displayed more of AF-like characteristics. The addition of GDF5 to TGF-β1 mainly positively affected the anabolic gene expression of the MSCs but showed no impact on enhanced NP-like cell differentiation than TGF-β1 alone. Overall, although further improvements and investigations need to be made on the silk scaffolds, characteristics of an NP-like and AF-like tissue are present. Therefore, we believe that the here proposed silk constructs and the knowledge gained from this study opens new possibilities how tissue engineered approaches can be used to regenerate damaged and/or degenerated IVDs.

Acknowledgements

First, the authors would like to thank Andrea Oberli for technical support. Then we thank Stefan Bracher, Benjamin Voumard and Philippe Zysset for answering any questions related to the biomechanical aspects of the scaffolds. Finally, we would like to thank Sonja Häckel, Katharina Oswald, Sebastian Bigdon, and Christoph Albers for providing human bone marrow aspirations from patients.

Author contributions

A. Croft: conceptualization, methodology, investigation, original draft preparation, data acquisition
J. Fuhrer: investigation, original draft preparation, data acquisition
M. Wöltje: conceptualization, resources, review and editing, funding acquisition
B. Gantenbein: conceptualization, resources, review and editing, funding acquisition, supervision

Ethics approval and consent to participate

All patients provided written consent, and the procedure was approved by the ethics committee of the Canton of Bern (with either of the two valid ethical permissions: either SwissEthics #2019-00097, or the general consent of the Insel University Hospital, respectively).

Funding

This study was supported by the Swiss National Science Foundation (project #310030E_192674/1, https://data.snf.ch/grants/grant/192674, accessed on 22 July 2023) and by the Deutsche Forschungsgemeinschaft (DFG, German Research Foundation #437213841).

Conflict of interest

The authors declare no conflict of interest.

References

Acaroglu ER, Iatridis JC, Setton LA, Foster RJ, Mow VC, Weidenbaum M (1995) Degeneration and aging affect the tensile behavior of human lumbar anulus fibrosus. Spine (Phila Pa 1976) **20**: 2690-2701. DOI: 10.1097/00007632-199512150-00010.

Adams MA, Roughley PJ (2006) What is intervertebral disc degeneration, and what causes it? Spine (Phila Pa 1976) **31**: 2151-2161. DOI: 10.1097/01.brs.0000231761.73859.2c.

Adams P, Eyre DR, Muir H (1977) Biochemical aspects of development and ageing of human lumbar intervertebral discs. Rheumatol Rehabil **16**: 22-29. DOI: 10.1093/rheumatology/16.1.22.

Altman GH, Diaz F, Jakuba C, Calabro T, Horan RL, Chen J, Lu H, Richmond J, Kaplan DL (2003) Silk-based biomaterials. Biomaterials **24**: 401-416. DOI: 10.1016/s0142-9612(02)00353-8.

Berthiaume F, Maguire TJ, Yarmush ML (2011) Tissue engineering and regenerative medicine: history, progress, and challenges. Annu Rev Chem Biomol Eng **2**: 403-430. DOI: 10.1146/annurev-chembioeng-061010-114257.

Bhattacharjee M, Miot S, Gorecka A, Singha K, Loparic M, Dickinson S, Das A, Bhavesh NS, Ray AR, Martin I, Ghosh S (2012) Oriented lamellar silk fibrous scaffolds to drive cartilage matrix orientation: towards annulus fibrosus tissue engineering. Acta Biomater **8**: 3313-3325. DOI: 10.1016/j.actbio.2012.05.023.

Bhunia BK, Kaplan DL, Mandal BB (2018) Silk-based multilayered angle-ply annulus fibrosus construct to recapitulate form and function of the intervertebral disc. Proc Natl Acad

Sci U S A **115**: 477-482. DOI: 10.1073/pnas.1715912115.

Brinjikji W, Diehn FE, Jarvik JG, Carr CM, Kallmes DF, Murad MH, Luetmer PH (2015) MRI Findings of Disc Degeneration are More Prevalent in Adults with Low Back Pain than in Asymptomatic Controls: A Systematic Review and Meta-Analysis. AJNR Am J Neuroradiol **36**: 2394-2399. DOI: 10.3174/ajnr.A4498.

Brown J, Lu CL, Coburn J, Kaplan DL (2015) Impact of silk biomaterial structure on proteolysis. Acta Biomater **11**: 212-221. DOI: 10.1016/j.actbio.2014.09.013.

Chen AX, Hoffman MD, Chen CS, Shubin AD, Reynolds DS, Benoit DS (2015) Disruption of cell-cell contact-mediated notch signaling via hydrogel encapsulation reduces mesenchymal stem cell chondrogenic potential: winner of the Society for Biomaterials Student Award in the Undergraduate Category, Charlotte, NC, April 15 to 18, 2015. J Biomed Mater Res A **103**: 1291-1302. DOI: 10.1002/jbm.a.35383.

Chujo T, An HS, Akeda K, Miyamoto K, Muehleman C, Attawia M, Andersson G, Masuda K (2006) Effects of Growth Differentiation Factor-5 on the Intervertebral Disc–In Vitro Bovine Study and In Vivo Rabbit Disc Degeneration Model Study. Spine **31**: 2909-2917. DOI: 10.1097/01.brs.0000248428.22823.86.

Clarke LE, McConnell JC, Sherratt MJ, Derby B, Richardson SM, Hoyland JA (2014) Growth differentiation factor 6 and transforming growth factor-beta differentially mediate mesenchymal stem cell differentiation, composition, and micromechanical properties of nucleus pulposus constructs. Arthritis Res Ther **16**: R67. DOI: 10.1186/ar4505.

Colombier P, Clouet J, Boyer C, Ruel M, Bonin G, Lesoeur J, Moreau A, Fellah BH, Weiss P, Lescaudron L, Camus A, Guicheux J (2016) TGF-beta1 and GDF5 Act Synergistically to Drive the Differentiation of Human Adipose Stromal Cells toward Nucleus Pulposus-like Cells. Stem Cells **34**: 653-667. DOI: 10.1002/stem.2249.

Costa JB, Silva-Correia J, Ribeiro VP, da Silva Morais A, Oliveira JM, Reis RL (2019) Engineering patient-specific bioprinted constructs for treatment of degenerated intervertebral disc. Mater Today Commun **19**: 506-512. DOI: 10.1016/j.mtcomm.2018.01.011.

Croft AS, Spessot E, Bhattacharjee P, Yang Y, Motta A, Woltje M, Gantenbein B (2022) Biomedical applications of silk and its role for intervertebral disc repair. JOR Spine **5**: e1225. DOI: 10.1002/jsp2.1225.

Dagenais S, Caro J, Haldeman S (2008) A systematic review of low back pain cost of illness studies in the United States and internationally. Spine J **8**: 8-20. DOI: 10.1016/j.spinee.2007.10.005.

Deyo RA, Weinstein JN (2001) Low back pain. N Engl J Med **344**: 363-370. DOI: 10.1056/NEJM200102013440508.

Du J, Guo W, Hackel S, Hoppe S, Garcia JP, Alini M, Tryfonidou MA, Creemers LB, Grad S, Li Z (2022) The function of CD146 in human annulus fibrosus cells and mechanism of the regulation by TGF-beta. J Orthop Res **40**: 1661-1671. DOI: 10.1002/jor.25190.

Elliott DM, Setton LA (2001) Anisotropic and inhomogeneous tensile behavior of the human anulus fibrosus: experimental measurement and material model predictions. J Biomech Eng **123**: 256-263. DOI: 10.1115/1.1374202.

Eyre DR, Muir H (1976) Types I and II collagens in intervertebral disc. Interchanging radial distributions in annulus fibrosus. Biochem J **157**: 267-270. DOI: 10.1042/bj1570267.

Feng Q, Gao H, Wen H, Huang H, Li Q, Liang M, Liu Y, Dong H, Cao X (2020) Engineering the cellular mechanical microenvironment to regulate stem cell chondrogenesis: Insights from a microgel model. Acta Biomater **113**: 393-406. DOI: 10.1016/j.actbio.2020.06.046.

Ferreira ML, de Luca K, Haile LM, Steinmetz JD, Culbreth GT, Cross M, Kopec JA, Ferreira PH, Blyth FM, Buchbinder R, Hartvigsen J, Wu A-M, Safiri S, Woolf AD, Collins GS, Ong KL, Vollset SE, Smith AE, Cruz JA, Fukutaki KG, Abate SM, Abbasifard M, Abbasi-Kangevari M, Abbasi-Kangevari Z, Abdelalim A, Abedi A, Abidi H, Adnani QES, Ahmadi A, Akinyemi RO, Alamer AT, Alem AZ, Alimohamadi Y, Alshehri MA, Alshehri MM, Alzahrani H, Amini S, Amiri S, Amu H, Andrei CL, Andrei T, Antony B, Arabloo J, Arulappan J, Arumugam A, Ashraf T, Athari SS, Awoke N, Azadnajafabad S, Bärnighausen TW, Barrero LH, Barrow A, Barzegar A, Bearne LM, Bensenor IM, Berhie AY, Bhandari BB, Bhojaraja VS, Bijani A, Bodicha BBA, Bolla SR, Brazo-Sayavera J, Briggs AM, Cao C,

Charalampous P, Chattu VK, Cicuttini FM, Clarsen B, Cuschieri S, Dadras O, Dai X, Dandona L, Dandona R, Dehghan A, Demie TGG, Denova-Gutiérrez E, Dewan SMR, Dharmaratne SD, Dhimal ML, Dhimal M, Diaz D, Didehdar M, Digesa LE, Diress M, Do HT, Doan LP, Ekholuenetale M, Elhadi M, Eskandarieh S, Faghani S, Fares J, Fatehizadeh A, Fetensa G, Filip I, Fischer F, Franklin RC, Ganesan B, Gemeda BNB, Getachew ME, Ghashghaee A, Gill TK, Golechha M, Goleij P, Gupta B, Hafezi-Nejad N, Haj-Mirzaian A, Hamal PK, Hanif A, Harlianto NI, Hasani H, Hay SI, Hebert JJ, Heidari G, Heidari M, Heidari-Soureshjani R, Hlongwa MM, Hosseini M-S, Hsiao AK, Iavicoli I, Ibitoye SE, Ilic IM, Ilic MD, Islam SMS, Janodia MD, Jha RP, Jindal HA, Jonas JB, Kabito GG, Kandel H, Kaur RJ, Keshri VR, Khader YS, Khan EA, Khan MJ, Khan MAB, Khayat Kashani HR, Khubchandani J, Kim YJ, Kisa A, Klugarová J, Kolahi A-A, Koohestani HR, Koyanagi A, Kumar GA, Kumar N, Lallukka T, Lasrado S, Lee W-C, Lee YH, Mahmoodpoor A, Malagón-Rojas JN, Malekpour M-R, Malekzadeh R, Malih N, Mehndiratta MM, Mehrabi Nasab E, Menezes RG, Mentis A-FA, Mesregah MK, Miller TR, Mirza-Aghazadeh-Attari M, Mobarakabadi M, Mohammad Y, Mohammadi E, Mohammed S, Mokdad AH, Momtazmanesh S, Monasta L, Moni MA, Mostafavi E, Murray CJL, Nair TS, Nazari J, Nejadghaderi SA, Neupane S, Neupane Kandel S, Nguyen CT, Nowroozi A, Okati-Aliabad H, Omer E, Oulhaj A, Owolabi MO, Panda-Jonas S, Pandey A, Park E-K, Pawar S, Pedersini P, Pereira J, Peres MFP, Petcu I-R, Pourahmadi M, Radfar A, Rahimi-Dehgolan S, Rahimi-Movaghar V, Rahman M, Rahmani AM, Rajai N, Rao CR, Rashedi V, Rashidi M-M, Ratan ZA, Rawaf DL, Rawaf S, Renzaho AMN, Rezaei N, Rezaei Z, Roever L, Ruela GdA, Saddik B, Sahebkar A, Salehi S, Sanmarchi F, Sepanlou SG, Shahabi S, Shahrokhi S, Shaker E, Shamsi M, Shannawaz M, Sharma S, Shaygan M, Sheikhi RA, Shetty JK, Shiri R, Shivalli S, Shobeiri P, Sibhat MM, Singh A, Singh JA, Slater H, Solmi M, Somayaji R, Tan K-K, Thapar R, Tohidast SA, Valadan Tahbaz S, Valizadeh R, Vasankari TJ, Venketasubramanian N, Vlassov V, Vo B, Wang Y-P, Wiangkham T, Yadav L, Yadollahpour A, Yahyazadeh Jabbari SH, Yang L, Yazdanpanah F, Yonemoto N, Younis MZ, Zare I, Zarrintan A, Zoladl M, Vos T, March LM (2023) Global, regional, and national burden of low back pain, 1990–2020, its attributable risk factors, and projections to 2050: a systematic analysis of the Global Burden of Disease Study 2021. The Lancet Rheumatology **5**: e316-e329. DOI: 10.1016/S2665-9913(23)00098-X.

Frauchiger DA, Heeb SR, May RD, Woltje M, Benneker LM, Gantenbein B (2018a) Differentiation of MSC and annulus fibrosus cells on genetically engineered silk fleece-membrane-composites enriched for GDF-6 or TGF-beta3. J Orthop Res **36**: 1324-1333. DOI: 10.1002/jor.23778.

Frauchiger DA, May RD, Bakirci E, Tekari A, Chan SCW, Woltje M, Benneker LM, Gantenbein B (2018b) Genipin-Enhanced Fibrin Hydrogel and Novel Silk for Intervertebral Disc Repair in a Loaded Bovine Organ Culture Model. J Funct Biomater **9**: 40. DOI: 10.3390/jfb9030040.

Gantenbein-Ritter B, Benneker LM, Alini M, Grad S (2011) Differential response of human bone marrow stromal cells to either TGF-β1 or rhGDF-5. European Spine Journal **20**: 962-971. DOI: 10.1007/s00586-010-1619-z.

Green TP, Adams MA, Dolan P (1993) Tensile properties of the annulus fibrosus II. Ultimate tensile strength and fatigue life. Eur Spine J **2**: 209-214. DOI: 10.1007/BF00299448.

Hallett SA, Ono W, Ono N (2021) The hypertrophic chondrocyte: To be or not to be. Histol Histopathol **36**: 1021-1036. DOI: 10.14670/HH-18-355.

Hild M, Brünler R, Jäger M, Laourine E, Scheid L, Haupt D, Aibibu D, Cherif C, Hanke T (2014) Net Shape Nonwoven: a novel technique for porous three-dimensional nonwoven hybrid scaffolds. Textile Research Journal **84**: 1084-1094. DOI: 10.1177/0040517513515315.

Hoy D, Bain C, Williams G, March L, Brooks P, Blyth F, Woolf A, Vos T, Buchbinder R (2012) A systematic review of the global prevalence of low back pain. Arthritis Rheum **64**: 2028-2037. DOI: 10.1002/art.34347.

Hu J, Lu Y, Cai L, Owusu-Ansah KG, Xu G, Han F, Bao J, Lin X, Huang Y (2017) Functional compressive mechanics and tissue biocompatibility of an injectable SF/PU hydrogel for nucleus pulposus replacement. Sci Rep **7**: 2347. DOI: 10.1038/s41598-017-02497-3.

Iatridis JC, MacLean JJ, O'Brien M, Stokes IA (2007) Measurements of proteoglycan and water content distribution in human lumbar

intervertebral discs. Spine (Phila Pa 1976) **32**: 1493-1497. DOI: 10.1097/BRS.0b013e318067dd3f.

Inoue H, Takeda T (1975) Three-dimensional observation of collagen framework of lumbar intervertebral discs. Acta Orthop Scand **46**: 949-956. DOI: 10.3109/17453677508989283.

Li M, Ogiso M, Minoura N (2003) Enzymatic degradation behavior of porous silk fibroin sheets. Biomaterials **24**: 357-365. DOI: 10.1016/s0142-9612(02)00326-5.

Livak KJ, Schmittgen TD (2001) Analysis of relative gene expression data using real-time quantitative PCR and the 2(-Delta Delta C(T)) Method. Methods **25**: 402-408. DOI: 10.1006/meth.2001.1262.

Lv B, Gan W, Cheng Z, Wu J, Chen Y, Zhao K, Zhang Y (2022) Current Insights Into the Maintenance of Structure and Function of Intervertebral Disc: A Review of the Regulatory Role of Growth and Differentiation Factor-5. Front Pharmacol **13**: 842525. DOI: 10.3389/fphar.2022.842525.

Maroudas A, Stockwell RA, Nachemson A, Urban J (1975) Factors involved in the nutrition of the human lumbar intervertebral disc: cellularity and diffusion of glucose in vitro. J Anat **120**: 113-130.

Minogue BM, Richardson SM, Zeef LA, Freemont AJ, Hoyland JA (2010) Characterization of the human nucleus pulposus cell phenotype and evaluation of novel marker gene expression to define adult stem cell differentiation. Arthritis Rheum **62**: 3695-3705. DOI: 10.1002/art.27710.

Mueller MB, Fischer M, Zellner J, Berner A, Dienstknecht T, Prantl L, Kujat R, Nerlich M, Tuan RS, Angele P (2010) Hypertrophy in mesenchymal stem cell chondrogenesis: effect of TGF-beta isoforms and chondrogenic conditioning. Cells Tissues Organs **192**: 158-166. DOI: 10.1159/000313399.

Nerurkar NL, Baker BM, Sen S, Wible EE, Elliott DM, Mauck RL (2009) Nanofibrous biologic laminates replicate the form and function of the annulus fibrosus. Nat Mater **8**: 986-992. DOI: 10.1038/nmat2558.

O'Connell GD, Sen S, Elliott DM (2012) Human annulus fibrosus material properties from biaxial testing and constitutive modeling are altered with degeneration. Biomech Model Mechanobiol **11**: 493-503. DOI: 10.1007/s10237-011-0328-9.

Oichi T, Taniguchi Y, Oshima Y, Tanaka S, Saito T (2020) Pathomechanism of intervertebral disc degeneration. JOR Spine **3**: e1076. DOI: 10.1002/jsp2.1076.

Park SH, Gil ES, Cho H, Mandal BB, Tien LW, Min BH, Kaplan DL (2012a) Intervertebral disk tissue engineering using biphasic silk composite scaffolds. Tissue Eng Part A **18**: 447-458. DOI: 10.1089/ten.TEA.2011.0195.

Park SH, Gil ES, Mandal BB, Cho H, Kluge JA, Min BH, Kaplan DL (2012b) Annulus fibrosus tissue engineering using lamellar silk scaffolds. J Tissue Eng Regen Med **6 Suppl 3**: s24-s33. DOI: 10.1002/term.541.

Pelttari K, Winter A, Steck E, Goetzke K, Hennig T, Ochs BG, Aigner T, Richter W (2006) Premature induction of hypertrophy during in vitro chondrogenesis of human mesenchymal stem cells correlates with calcification and vascular invasion after ectopic transplantation in SCID mice. Arthritis Rheum **54**: 3254-3266. DOI: 10.1002/art.22136.

Peng Y, Qing X, Lin H, Huang D, Li J, Tian S, Liu S, Lv X, Ma K, Li R, Rao Z, Bai Y, Chen S, Lei M, Quan D, Shao Z (2021) Decellularized Disc Hydrogels for hBMSCs tissue-specific differentiation and tissue regeneration. Bioact Mater **6**: 3541-3556. DOI: 10.1016/j.bioactmat.2021.03.014.

Risbud MV, Schoepflin ZR, Mwale F, Kandel RA, Grad S, Iatridis JC, Sakai D, Hoyland JA (2015) Defining the phenotype of young healthy nucleus pulposus cells: recommendations of the Spine Research Interest Group at the 2014 annual ORS meeting. J Orthop Res **33**: 283-293. DOI: 10.1002/jor.22789.

Salonius E, Kontturi L, Laitinen A, Haaparanta AM, Korhonen M, Nystedt J, Kiviranta I, Muhonen V (2020) Chondrogenic differentiation of human bone marrow-derived mesenchymal stromal cells in a three-dimensional environment. J Cell Physiol **235**: 3497-3507. DOI: 10.1002/jcp.29238.

See EY, Toh SL, Goh JC (2011) Effects of radial compression on a novel simulated intervertebral disc-like assembly using bone marrow-derived mesenchymal stem cell cell-sheets for annulus fibrosus regeneration. Spine (Phila Pa 1976) **36**: 1744-1751. DOI: 10.1097/brs.0b013e31821986b3.

Skaggs DL, Weidenbaum M, Iatridis JC, Ratcliffe A, Mow VC (1994) Regional variation in tensile properties and biochemical composition of the human lumbar anulus fibrosus. Spine (Phila Pa 1976) **19**: 1310-1319. DOI: 10.1097/00007632-199406000-00002.

Wagner DR, Lotz JC (2004) Theoretical model and experimental results for the nonlinear elastic behavior of human annulus fibrosus. J Orthop Res **22**: 901-909. DOI: 10.1016/j.orthres.2003.12.012.

Wöltje M, Künzelmann L, Belgücan B, Croft AS, Voumard B, Bracher S, Zysset P, Gantenbein B, Cherif C, Aibibu D (2023) Textile Design of an Intervertebral Disc Replacement Device from Silk Yarn. Biomimetics **8**: 152. DOI: 10.3390/biomimetics8020152.

Wuertz K, Godburn K, Iatridis JC (2009) MSC response to pH levels found in degenerating intervertebral discs. Biochem Biophys Res Commun **379**: 824-829. DOI: 10.1016/j.bbrc.2008.12.145.

Wuertz K, Godburn K, Neidlinger-Wilke C, Urban J, Iatridis JC (2008) Behavior of Mesenchymal Stem Cells in the Chemical Microenvironment of the Intervertebral Disc. Spine **33**: 1843-1849. DOI: 10.1097/BRS.0b013e31817b8f53.

Yang Y, Chen J, Migliaresi C, Motta A (2020) Natural Fibrous Protein for Advanced Tissue Engineering Applications: Focusing on Silk Fibroin and Keratin. Adv Exp Med Biol **1249**: 39-49. DOI: 10.1007/978-981-15-3258-0_3.

Zeng C, Yang Q, Zhu M, Du L, Zhang J, Ma X, Xu B, Wang L (2014) Silk fibroin porous scaffolds for nucleus pulposus tissue engineering. Mater Sci Eng C Mater Biol Appl **37**: 232-240. DOI: 10.1016/j.msec.2014.01.012.

Zhang T, Du L, Zhao J, Ding J, Zhang P, Wang L, Xu B (2020) Biomimetic angle-ply multi-lamellar scaffold for annulus fibrosus tissue engineering. J Mater Sci Mater Med **31**: 67. DOI: 10.1007/s10856-020-06404-7.

Editor's note: The Scientific Editor responsible for this paper was Sibylle Grad.